Chapter 39

Retinal Laser Therapy: Biophysical Basis and Applications

Daniel Palanker, Mark S. Blumenkranz

INTRODUCTION

Historically, a number of light sources have been utilized for retinal phototherapy, including the sun, various flash lamps, and lasers. The sun is capable of producing a retinal burn either accidentally (e.g., in the case of solar eclipse retinopathy) or on purpose, as demonstrated first by Meyer-Schwickerath.[1] However, its dependence on weather conditions, its constant motion in the sky, and relatively large angular size (0.52°) make it an impractical method for intraocular therapy.

Arc lamps are very bright sources of light used in many therapeutic and imaging applications. In such lamps, a high-voltage discharge initially ionizes gas between an anode and cathode, creating an electric arc – a high-current-density discharge in the lamp. The ions emit light at specific wavelengths, and the spectrum of the plasma emission depends on the types of atoms involved, their temperatures, and gas pressure. Thus the spectrum of an arc lamp may have a distinct signature. The xenon arc lamp was the first to become widely used for retinal photocoagulation because of its strong visible and near-infrared emission, convenience, and low price. However, because of its large size and tendency to produce intense retinal burns, it was replaced in clinical practice by laser-based systems in the early 1970s.[2]

Lasers became the preferred light source for retinal photocoagulation due their narrow spectrum, wide selection of wavelengths, excellent collimation (directionality), high brightness, and variable pulse duration. The directionality of the laser makes it easy to manipulate the beam optically before its introduction into the eye, and to focus it into very small spots. Its monochromaticity makes it possible to choose a wavelength for selective absorption in specific tissues of the eye. Adjustable pulse duration allows limiting the thermal diffusion to small distances, thus producing very precise and selective interactions with minimal collateral damage.

The most widespread medical applications of lasers in medicine have been in ophthalmology. Since the introduction of the ruby laser more than three decades ago, ophthalmic laser applications have experienced rapid growth with the use of argon, krypton, argon-pumped dye, Nd:YAG, diode, Er:YAG, excimer, and Ti:sapphire lasers. Lasers have been applied to a wide variety of slit-lamp-based retinal therapies, as well as to vitreoretinal surgery, glaucoma, lens capsule opacification, and refractive surgery. These applications are based on different mechanisms of laser–tissue interactions including photothermal, photodisruptive, and photochemical interactions. The most common vitreoretinal application is retinal photocoagulation. Additionally, a number of novel therapies have recently been introduced and are under active evaluation, including selective retinal pigment epithelium (RPE) treatment and sublethal thermal therapy.

In the following sections we will describe the underlying principles of laser–tissue interactions and the types of lasers available and appropriate for various vitreoretinal applications.

Optical properties of the eye

The relaxed eye has an approximate optical power of 60 D (i.e., its focal length is 16.7 mm in air), with the corneal power being about 40 D, or two-thirds of the total power.[3] Due to orderly arrangement of collagen fibrils in the cornea it is highly transparent, with transmission above 95% in the spectral range of 400–900 nm.[4] The refractive index of the cornea is $n \approx 1.3765 \pm 0.0005$.[4] The amount of light reaching the retina is regulated by the pupil size, which can vary between 1.5 and 8 mm. The anterior chamber of the eye, which is located between the cornea and lens capsule, is filled with a clear liquid – the aqueous humor, which has a refractive index $n \approx 1.3335$. The crystalline lens of the eye, located behind the iris, is composed of specialized crystallin proteins with refractive index of $n = 1.40–1.42$. The lens is about 4 mm in thickness and 10 mm in diameter and is enclosed in a tough, thin (5–15 μm), transparent collagenous capsule. In the relaxed eye the lens has a power of about 20 D, while in the fully accommodated state it can temporarily increase to 33 D. The vitreous humor, a transparent jelly-like substance filling the large cavity posterior to the lens, and anterior to the retina, has a refractive index $n \approx 1.335$.[4]

Light entering the eye can be reflected, scattered, transmitted, or absorbed. Reflected or scattered light contains information that can be used for noninvasive diagnostic purposes. The absorption characteristics of ocular tissues are determined by the chromophores resident within the tissue. In the visible part of the spectrum (400–800 nm) these chromophores include: (1) melanin located in the retinal and iris pigmented epithelia, choroid, uvea, and trabecular meshwork; (2) hemoglobin, located in the red blood cells; (3) macular xanthophyl, which is located in the plexiform layers of the retina, especially near and in the macula; (4) rhodopsin and cone photopigments which are located in the photoreceptors; and (5) lipofuscin, located primarily in the RPE layer. These pigments are of major importance in absorption of visible light in the retina from both physiologic and pathologic standpoints. The absorption spectra of these pigments, as well as water and proteins, are illustrated in Figure 39.1. In the mid-infrared part of the spectrum (3–15 μm) the major absorber is water, while in ultraviolet (below 250 nm) protein absorption is dominant.

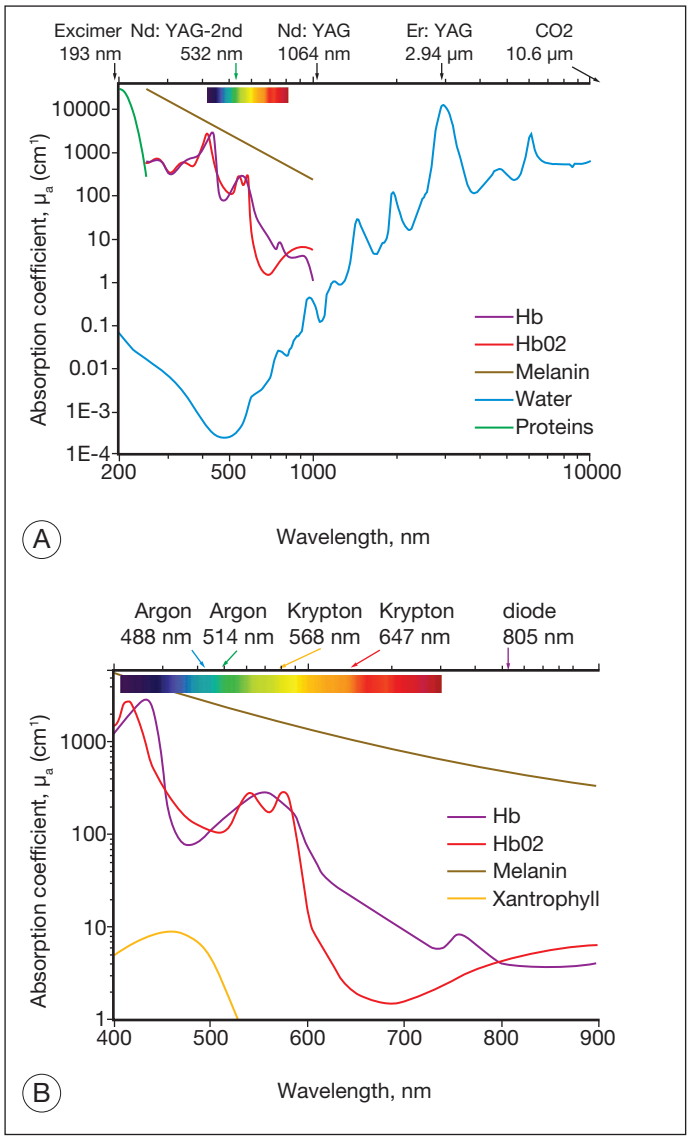

Fig. 39.1 (A) Absorption coefficients for major chromophores in a spectral range of 0.2–10 µm. (B) Absorption coefficients of the major ocular chromophores in the visible part of the spectrum: 400–900 nm. Spectral locations of some of the popular laser lines in this range are indicated above the plots.

BASICS OF LASERS

The term "laser" stands for light amplification by stimulated emission of radiation. A beam of light is composed of individual packets of energy that are called quanta or photons. Each of these photons has a particular energy and direction of travel. The energy of a quantum of light is proportional to its frequency, i.e., it is reciprocal of its wavelength. In the presence of a properly prepared laser material, it is possible for a quantum of light to trigger the release of other quanta with the same wavelength and direction of travel. This phenomenon is called stimulated emission, and it is an essential element in lasing. In thermal equilibrium the energy levels of atoms and molecules are populated according to the Boltzmann distribution, in which upper levels are always less populated than the lower levels. Stimulated emission requires an inverted population of energy levels, such that the upper levels are more populated than the lower ones. As a result, lasing can occur only when material is not in thermal equilibrium. The nonequilibrium state is created in the lasing material by an excitation source or "pump."

Generally, a laser is composed of three basic components: (1) a material that can store energy to be released by stimulated emission; (2) a means of replenishing the energy stored in the lasing material; and (3) some method of retaining a fraction of the light emitted by the lasing material to stimulate further emission. Figure 39.2 schematically illustrates a general configuration of a laser. An energy source is used to introduce energy into the lasing material. This energy is stored as atomic or molecular excitation waiting to be released by stimulated emission. Laser light that has already been emitted by the lasing material circulates between the two mirrors on either end of the laser cavity, with a fraction of the light escaping through one mirror to form the laser beam. The trapped light stimulates emission of new quanta of light from the laser material with the same wavelength and direction as the original quanta. In this way, a laser produces a beam of light between the two mirrors in which all of the quanta move in phase with one another. This property of light is called coherence.

Coherence is related to synchronization of light in time, or along the laser beam. The duration of the synchronized emission from the laser multiplied by the speed of light is called the coherence length of the laser emission. This is the distance along

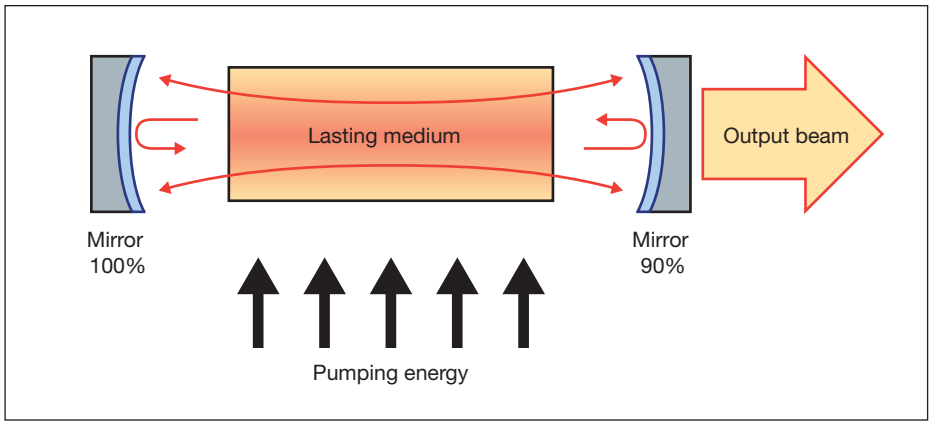

Fig. 39.2 Laser typically consists of the energy source (pump), the lasing medium, and the optical cavity with a partially transparent front mirror.

which the photons are coherent, or moving "in step." To remain in phase with one another, these quanta must have approximately the same wavelength. Thus temporal coherence is related to the monochromaticity (or spectral width) of the light emitted from the laser: the broader the spectrum, the shorter the temporal coherence. A laser may produce one or several discrete spectral lines in the infrared, visible, or ultraviolet domains, in contrast to conventional light sources (incandescent or arc lamps) which typically produce noncoherent polychromatic (broadband or white) light.

Collimation (directionality) of the emitted beam is governed by the mirror configuration of the laser cavity. In its simplest form, a cavity consists of two mirrors arranged such that light bounces back and forth, each time passing through the gain medium. One of the two mirrors, the output coupler, is partially transparent, allowing the output beam to exit through it (Fig. 39.2). The reflection coefficient of the output coupler determines how many times photons are reflected back to circulate inside the cavity before exiting it. For example, with a reflection coefficient of 0.99, the photon will bounce, on average, 99 times before exiting the cavity. The structure of the laser cavity determines directionality (collimation) of the laser beam, which determines its ability to be focused into a small spot.

The lasing medium can be a gas, liquid, or solid. Lasers can be pumped by continuous discharge lamps and by pulsed flash lamps, by electric discharges in the laser medium, by chemical reactions, by an electron beam, by direct conversion of electric current into photons in semiconductors, or by light from other lasers. Laser pulse durations can vary from femtoseconds to infinity. Pulsing techniques used for different ranges of pulse durations include electronic shutters (down to 1 ms), pulsed flash lamps (typically down to a few μs), Q-switching (down to a few ns), or mode-locking (down to fs).

Laser beam delivery to tissue

Laser beams are typically very well collimated. Diffraction causes light waves to spread transversely as they propagate, and it is therefore impossible to have a perfectly collimated beam. The diffraction-limited divergence angle of a gaussian beam with diameter D and wavelength λ is $\Theta = \frac{4 \cdot \lambda}{\pi \cdot D}$. As an example, for an argon laser emitting a 1-mm-wide beam at 515 nm wavelength, the divergence (half-angle Θ) is about 0.66 mrad, i.e., the beam spreads by 1.3 mm over a distance of 1 meter.

Using a lens or a concave mirror with focal length f, a laser beam can be focused to a spot with a diameter $d = \frac{4 \cdot f}{\pi \cdot D}\lambda$. The depth of the focal region is $F = \frac{8 \cdot f^2}{\pi \cdot D^2}\lambda$ (Fig. 39.3). With a f = 25 mm lens the same argon laser beam can be focused to a spot of 16 μm in diameter, having a focal depth of 820 μm. It must be emphasized, though, that exact definition of the spot size depends on the beam profile, which varies in various configurations of laser cavities. For therapeutic laser photocoagulation such tight focusing is usually not required, and laser spots typically vary in diameter between 50 and 500 μm in various applications.

As an alternative to a free-propagating beam, laser light can be transported via optical fibers. An optical fiber, schematically shown in Figure 39.4, typically consists of a core, cladding, and jacket. Light is trapped within the core due to total internal reflection at the interface of core with cladding. To satisfy conditions of total internal reflection, the incidence angle of light at the core–cladding interface should not exceed the critical angle of total internal reflection: $\sin\Theta_{cr} = n_{core}/n_{clad}$, where n_{core} and n_{clad} are refractive indices of the core and cladding, respectively. To satisfy these criteria for total internal reflection, the light should

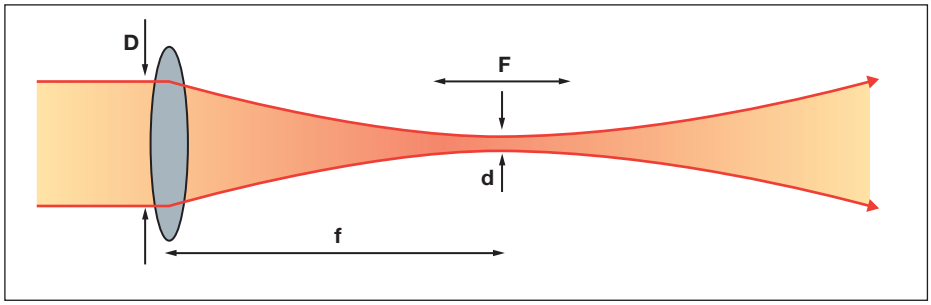

Fig. 39.3 Laser beam of diameter D focused with a lens of focal length f produces a waist with diameter d and a focal depth F (see equations in the text).

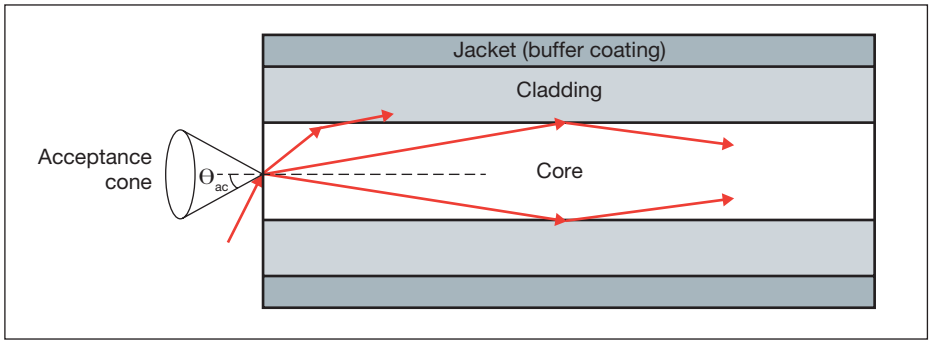

Fig. 39.4 Optical fiber typically consists of a core, cladding, and a jacket (buffer coating). Light launched into the fiber with its acceptance cone Θ_{ac} is trapped within a core due to the total internal reflection at the core–cladding interface.

Fig. 39.5 Laser photocoagulation on a slit-lamp system. 1, Optical fiber and electronic cable connecting laser with a slit-lamp system; 2, optical coupler projecting the beam exiting from the fiber on to the retina; 3, contact lens.

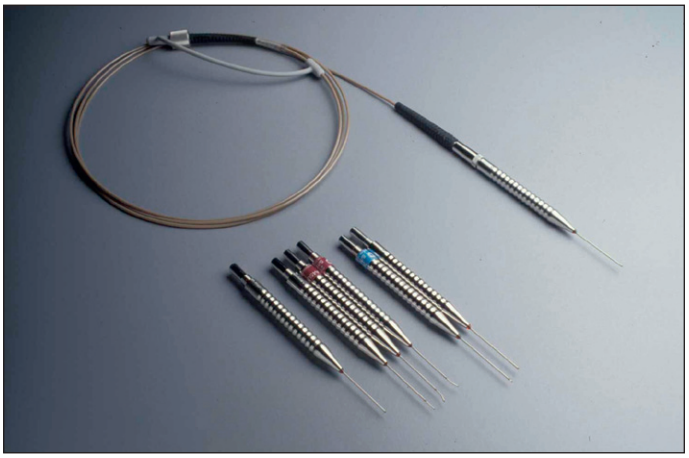

Fig. 39.6 Intraocular hand pieces and optical fiber for vitreoretinal dissection with the Er:YAG laser.

be launched within a so-called acceptance cone, and the sine of its half-angle Θ_{ac} is defined as the numerical aperture (NA) of the fiber: $NA = \sin\Theta_{ac} = \sqrt{n_{core}^2 - n_{clad}^2}$. Typically the NA is within a range of 0.1–0.2. Optical fibers are often used for delivery of laser light to slit-lamp-based systems (Fig. 39.5), and to intraocular surgical probes (Fig. 39.6).

ABERRATIONS

With nonperfect focusing optics, the focal spot size of the laser beam is limited not only by diffraction, but also by aberrations. Measurements of optical aberrations in the human eye demonstrate[5,6] that for pupillary dilation of up to 3 mm in diameter, an average emmetropic human eye is optically well corrected, and the focal spot is close to the diffraction limit. However, for pupils greater than 3 mm in diameter, central aberrations increase, resulting in increases in the focal spot size. Peripheral field aberrations lead to rapidly increasing blur of the image with angle of visual field, strongly limiting the focusing capability of laser in the periphery of the retina.[6] In retinal photocoagulation, a flat contact lens is typically used to reduce the optical power of the front surface of the cornea. If the lens is used properly it aids greatly in controlling peripheral aberrations during photocoagulation. Other methods include using an aspheric lens to control optical aberrations in the periphery during photocoagulation. The use of such lenses has many advantages, in particular for providing wide-field viewing, although aberrations are difficult to correct over the totality of fields of interest and additional reflections may be introduced by the lens surfaces.

Table 39.1 Ocular contact lenses and their magnifications in a human eye

Lens	Image magnification	Laser beam magnification
Ocular Mainster Standard	0.95	1.05
Ocular Fundus Laser	0.93	1.08
Ocular Mainster Wide Field	0.67	1.50
Ocular Mainster Ultra Mag	0.53	1.90
Ocular Mainster 165	0.51	1.96
Ocular Three Mirror Universal	0.93	1.08
Volk G-3 Gonio Fundus	1.06	0.94
Volk Area Centralis	1.06	0.94
Volk Trans Equator	0.69	1.44
Volk SuperQuad 160	0.5	2.00
Volk QuadrAspheric	0.51	1.97
Volk High Resolution Wide Field	0.5	2.00
Rodenstock Panfundoscope	0.67	1.50

CONTACT LENSES

Currently, retinal laser photocoagulation relies heavily on the use of contact lenses. A number of contact lenses have been developed for this purpose, and the most common types are listed in Table 39.1. The universal (Goldmann) three-mirror contact lens provides a flat front surface that nearly cancels the positive refractive power of the front surface of the cornea. Mirrors at 5°, 67°, and 73° aid in visualization and photocoagulation of the periphery and anterior segment. To obtain the most reproducible results in photocoagulation the operator should hold the contact lens so that the flat surface is within ±5° of perpendicular to the laser beam (Fig. 39.5). The use of mirrors in contact lenses helps the operator keep the laser beam properly aligned to the lens while photocoagulating over a large field.

Another useful photocoagulation lens is the inverted image lens system, typified by the Rodenstock, Quadraspheric, and

Mainster photocoagulation lenses. These lenses contain a lens element in contact with the corneal surface and another positive lens element at a fixed distance from the cornea. These systems magnify the spot size on the retina, while increasing the field of view, requiring the operator to adjust the power accordingly. Magnification factors of the most common contact lenses are listed in Table 39.1. It is important to keep in mind that magnification of the retinal image demagnifies the beam size on the retina by the same amount: the higher the magnification of the retina, the smaller the laser spot on the retina.

INTERACTIONS OF LIGHT WITH TISSUE

In linear interactions the irradiance (or power fluence) $I(z)$ (W/cm^2) of the beam propagating inside tissue decreases exponentially with depth (Beer's law) due to absorption and scattering of light: $I(z) = (1 - k_s)I_0\exp(-\mu z)$, where I_0 is the light intensity at the surface of tissue ($z = 0$), k_s is the specular reflection coefficient at the tissue surface, $\mu = \mu_a + \mu_s$ – is the attenuation coefficient, combined of absorption and scattering components. The penetration depth (δ) of the beam into tissue is defined as a depth at which light intensity is reduced by a factor of e: $\delta = 1/\mu$. Reflection of light from ocular tissue at normal incidence typically does not exceed 2%. As shown in Figure 39.1, absorption of light by various chromophores in the eye strongly varies with wavelength. Scattering of light is also a very strong function of the wavelength: scattering on subwavelength inhomogeneities of refractive index in ocular media (e.g., collagen fibrils) is reciprocal to the fourth power of the wavelength: $\mu_s \sim \lambda^{-4}$ (Rayleigh scattering). For example, the scattering coefficient for light at 1064 nm is 16 times lower than that at 532 nm. Scattering from structures larger than the wavelength (e.g., cellular organelles) is described by Mie theory and has more complex wavelength dependence and spatial distribution. Scaling of the Mie scattering coefficient with wavelength in various tissues can be approximated as $\mu_s \sim \lambda^{-b}$, with $b \approx 0.5–2$.[7,8]

Photochemical interactions

Photochemical interactions are based upon nonthermal light-induced chemical reactions. The best-known natural photochemical reactions are photosynthesis in plants and phototransduction in photoreceptors. Therapeutic photochemical interactions used in photodynamic therapy (PDT) take place at very low power densities (typically <1 W/cm^2) and long exposures – lasting tens of seconds. For PDT special chromophores, called photosensitizers, are injected intravenously and allowed to accumulate in the target tissues. After excitation by laser radiation the photosensitizer produces highly cytotoxic reactants – free radicals or singlet oxygen, which in turn produce irreversible oxidation of the targeted cell structures.

The concept of treating exudative age-related macular degeneration (AMD) by selectively targeting vascular endothelial cells using a specific photosensitizer–carrier complex (phthalocyanine, CASPc) activated by near-infrared laser was adapted from tumor therapy.[9,10] Closure of subretinal neovascularization using PDT with rose Bengal was demonstrated a few years later.[11] Following upon the successful initial results with phthalocyanine, liposomal benzoporphyrin derivative, which selectively attaches to the endothelium of new blood vessels was developed (verteporfin, or Visudyne).[12,13]

Clinical indication: photodynamic therapy for subfoveal choroidal neovascularization

PDT for subfoveal choroidal neovascularization (CNV) is performed as a two-step procedure. First, a specialized spectrally adapted photosensitizer, such as verteporfin, is injected intravenously into the patient. Within minutes it is distributed via the bloodstream to tissues, including the retina and choroid. It selectively accumulates in neovascular tissue which is rich in low-density lipoprotein receptors, while it is rapidly cleared from the surrounding normal tissues. This differential accumulation and clearance is the physicochemical basis for selectivity of PDT against neovascularization compared with the normal choroidal and retinal vasculature. The presence of increased numbers of new vessels in tumors has also led to the use of PDT as a treatment for several different ocular and nonocular tumors.

Upon absorption of a photon at the proper wavelength the porphyrin molecule undergoes an electronic transition from the ground state into the singlet excited state (^{1}P*). The singlet excited porphyrin can decay back to the ground state with release of energy in the form of fluorescence – enabling identification of tumor tissue (Fig. 39.7). The singlet can also be converted into the triplet excited state (^{3}P*) which is able to transfer energy to another triplet. One of the very few molecules with a triplet ground state is dioxygen, which is found in most cells. Energy transfer therefore takes place, producing toxic singlet oxygen ($^1O_2$) from ground-state dioxygen ($^3O_2$). Singlet oxygen is very reactive and thus it has a very short diffusion pathlength – less than 0.02 μm – so all its interactions are highly localized. The photochemical processes and subsequent reactions are complex and different for different sensitizers, and are also subject to the microenvironment. Singlet oxygen and other highly reactive species produced by photosensitizers damage endothelial cells in close proximity to the adsorbed drug, resulting in photothrombosis and temporary closure of the neovascularization.

Many photosensitizing dyes have been tested for PDT, including rose Bengal, hematoporphyrin derivatives, lutetium, texafrim, Photofrin, and various benzoporphyrins. Only verteporfin (Visudyne) has been approved for ophthalmic use in the

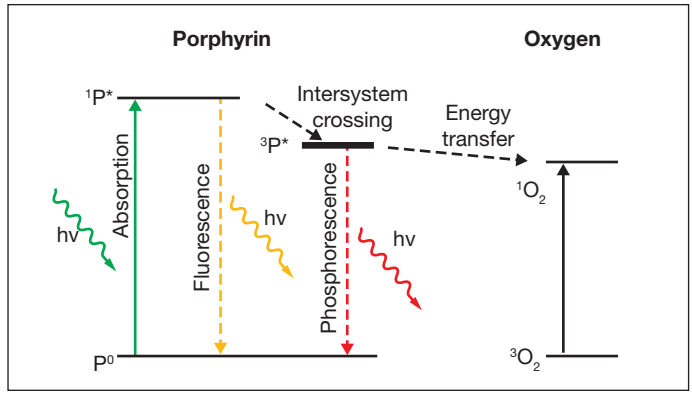

Fig. 39.7 Simplified diagram (with vibrational levels omitted) of the photoexcitation process in porphyrin and energy transfer to oxygen. Light causes excitation of porphyrin to the singlet excited state (^{1}P*). It can decay back to the ground state with release of fluorescence or convert into excited state (^{3}P*) which is able to transfer energy to a triplet ground state of oxygen. Such energy transfer results in highly toxic singlet oxygen ($^1O_2$).

treatment of classic and occult CNV. Verteporfin has a very broad absorption spectrum, but only the far-red peak at 688–691 nm is typically utilized in clinical practice (Fig. 39.8). This is because of the lower sensitivity of retina to far-red light and its superior penetration into the choroid.[14]

In PDT treatment with verteporfin activation by laser is typically performed 15–20 minutes after the intravenous injection of the dye. A beam of red laser light (689 nm diode laser) is applied to the retina via a slit-lamp delivery system, irradiating a spot chosen to exceed the dimension of the neovascularization minimally, with light intensity of 600 mW/cm^2, for 83 seconds, resulting in a total radiant exposure of 50 J/cm^2.[15,16] Closure of abnormal (leaking) blood vessels occurs for approximately 6–12 weeks in most patients. Reperfusion is common and multiple treatments are often required. Figures 39.9A (pretreatment) and 39.9B (1 week posttreatment) showing fluorescein angiography images demonstrate closure of a subfoveal CNV membrane after PDT.

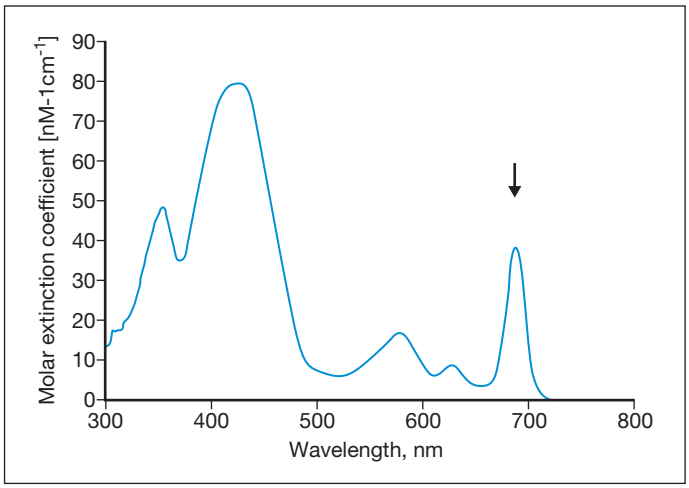

Fig. 39.8 Absorption spectrum of verteporfin. Arrow indicates the 689-nm peak typically used for photodynamic therapy.

Photothermal interactions

Temperature is the governing parameter in all thermal laser–tissue interactions. Depending on the duration and peak value of the temperature, different tissue effects, including necrosis, coagulation, vaporization, carbonization, and melting, may occur.

Heat generation in tissue is determined by the laser parameters and optical tissue properties – irradiance, exposure time, and the absorption coefficient, which is a function of the laser wavelength. Heat transport is characterized by heat conductivity and heat capacity. Heat effects depend on the type of tissue and temperature history (values and durations).

Absorption of light in tissue leads to heating. If heat diffusion is not taken into account, then at a constant beam intensity the temperature rise is linear with time: $T(z,t)=\frac{\mu_a \cdot I(z) \cdot t}{\rho \cdot c}$, where ρ is tissue density, and c is its heat capacity (c = 4.2 J/g/K, ρ = 1 g/cm^3 for water). To assess whether heat diffusion plays a significant role during the laser pulse, one should compare pulse duration with a characteristic time it takes for heat to spread by the distance equal to the zone of initial heat deposition in tissue. For the heated zone (laser penetration depth) of length L, the heat diffusion time is: $\tau = L^2/4\alpha$, where α is thermal diffusivity ($\alpha = 1.4 \cdot 10^{-3}$ cm^2/s for water). For example, for L = 1 μm in water the characteristic heat diffusion time is t = 1.7 μs, while for L = 1 mm the diffusion time t = 1.7 s. If the laser pulse duration is comparable or longer than the characteristic diffusion time across the light absorption zone, then proper estimation of the peak temperature in tissue should take heat diffusion into account.

Sublethal thermotherapy

There is a growing body of clinical evidence that diabetic macular edema can be successfully treated by pulsed near-infrared diode laser (810 nm) without producing visible lesions.[17–21] Using 300-ms bursts of submillisecond "micropulses," laser energy is applied with no visible lesions and no fluorescein leakage, as

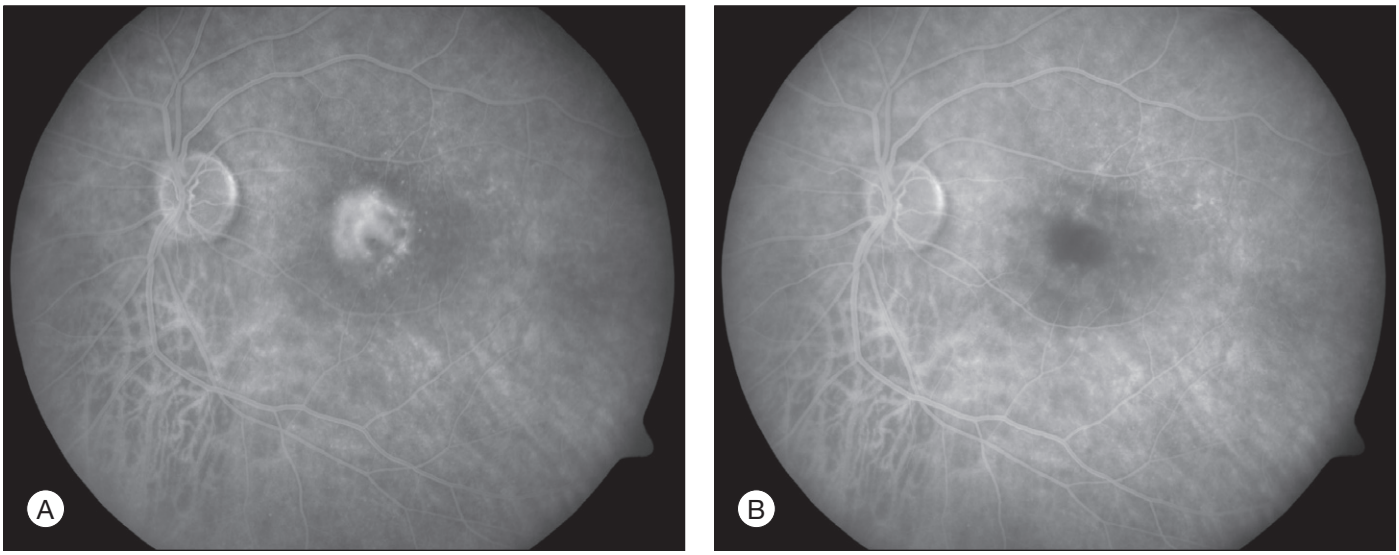

Fig. 39.9 (A) Fluorescein angiogram of a patient with predominantly occult subfoveal choroidal neovascular membrane in left eye. (B) Same eye 1 week following photodynamic therapy with verteporfin and intravitreal triamcinolone injection. Note absence of hyperfluorescence in the area of previous neovascularization and subtle darkening of choroid corresponding to area of photodynamic closure of the membrane.

observed acutely and in subsequent clinical exams. However, application of higher power can lead to significant heat accumulation and result in damage to RPE and photoreceptors.[17,22] Avoidance of acute laser-induced retinal damage permits applying this treatment confluently on the target retina with a large number of small (125 µm), densely placed laser spots.[19,23] The absence of damage allows this therapy to be repeated as necessary, and makes this technique potentially appealing in applications proximal to the fovea. However, due to the lack of reliable dosimetry and observable measures for such subvisible treatment, this technique is difficult to optimize, leading to potentially broad variability in the outcomes.

Necrosis

Temperature rises induce conformational changes in various proteins, which denature at characteristic rates specific to protein species. These thermal processes, which may eventually lead to cell necrosis, depend on both the temperature and duration of the hyperthermia. Thermal cellular damage in a millisecond regime can be approximated using the Arrhenius model.[24,25] It assumes a rate of decline in the concentration of a critical molecular component for cellular metabolism $D(t)$ with temperature $T(t)$:

$$dD(t) = -D(t) \cdot A \cdot \exp\left(-\frac{E^*}{R \cdot T(t)}\right) dt \qquad (1)$$

where E^* and A are the activation energy and rate constant setting parameters to the process, and R is the gas constant, 8.3 J/(K mol). Tissue damage, i.e., decrease in critical molecular component $D(\tau)$, relative to its initial value D_0 over the pulse length τ is encapsulated in the Arrhenius integral Ω:

$$\Omega(\tau) = -\ln\left(\frac{D(\tau)}{D_0}\right) = A\int_0^{\tau} \exp\left(-\frac{E^*}{R \cdot T(t)}\right) dt \qquad (2)$$

The model assumes that irreversible tissue damage takes place when concentration of the critical molecular component drops below some threshold value. Conventionally, this threshold corresponds to a reduction in concentration by a factor of e, or an Arrhenius integral of unity. Thus when $\Omega = 1$, the nondenatured fraction of proteins is $1/e \approx 37\%$, or in other words, 63% of proteins have been damaged.

Measurements of the RPE damage at various irradiation conditions yields the following average values[25]: E^* = 340 kJ/mol, $A = 1.6 \times 10^{55}$. It is important to keep in mind, though, that accurate estimation of cell survival under thermal stress is much more complex than just assessment of the denaturation rate of one type of protein or another. For example: (1) there are multiple types of proteins in cells and they denature at different rates; (2) different proteins have different importance for cellular survival; (3) cellular repair mechanisms cannot be ignored at long exposures. Therefore the single values of the reaction rate A and activation energy E most likely represent characteristics of the "weak link" in cellular metabolism, most susceptible to thermal damage.

Figure 39.10 shows an example of the temperature rise in tissue for a hypothetical square pulse of heating, which is sufficient for cell death, according to the Arrhenius model parameters listed above. Cells exposed to temperatures above the threshold curve are coagulated and the tissue becomes necrotic.

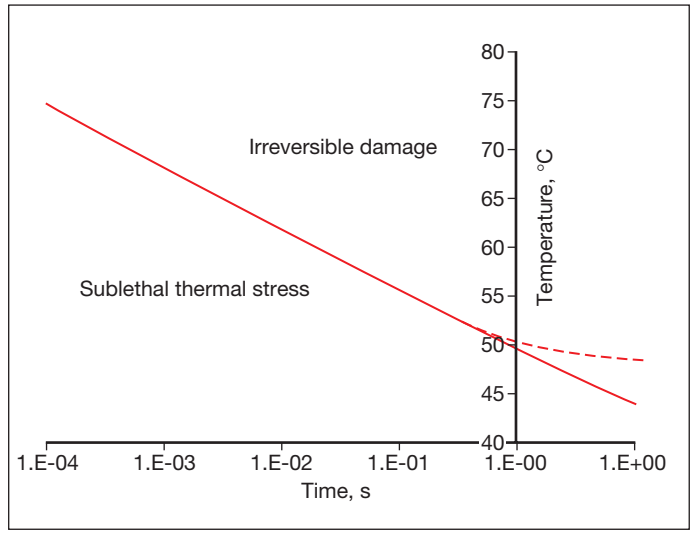

Fig. 39.10 Solid line depicts Arrhenius approximation of the cellular damage threshold as a function of duration of a hypothetical square pulse of heating. Dashed line indicates deviation of the damage threshold from the Arrhenius model at long exposures.

For example, at 1 second long exposure $T \approx 50$°C, while at 10 ms it requires 67°C for a lethal thermal damage. This curve is approximate, and the exact values depend on the shape of the actual pulse of temperature, type of cells, and tissues involved. The Arrhenius model fails to predict correct threshold temperatures at exposures longer than approximately 1 second, since cellular repair mechanisms should be taken into account at long exposures.

Transpupillary thermotherapy

The possibility of localized tissue coagulation and necrosis forms the basis of the tumor treatment technique called laser-induced interstitial thermotherapy (LITT) or transpupillary thermotherapy (TTT). It has been applied to tumors in retina, brain, prostate, and liver, and is considered a form of minimally invasive surgery. The concept of LITT is to apply a laser beam to tissue in such a way that the target tissue is heated for a prolonged period of time (about 1 minute) to temperatures above the threshold of necrosis (on the order of 60°C). To achieve deep penetration into tissue continuous wave lasers in the near-infrared region (800–1064 nm) are typically employed. TTT for the treatment of intraocular tumors[26] typically requires exposure times of 1 minute and irradiances varying from 5 to 12 W/cm^2.

The use of TTT has been tested in the treatment of CNV in AMD.[15,27,28] Proponents of this approach have hypothesized a selective effect on the heating of actively dividing cells in newly formed blood vessels due to their higher susceptibility to thermal injury than nondividing cells in normal tissue. The estimated retinal temperature elevation with TTT at standard settings (810 nm, 800 mW, 60 seconds, 3.0 mm spot size) is approximately 10°C.[29,30] The mechanism of treatment of CNV by TTT may occur through vascular thrombosis, apoptosis, or the thermal inhibition of angiogenesis.[31]

Photocoagulation

Retinal photocoagulation typically involves the application of laser pulses with durations ranging from 10 to 200 ms, and transient hyperthermia by tens of degrees above body temperature.

Various lasers have been used in the past (ruby (694 nm), argon (488, 514 nm), krypton (647 nm)). Currently the most common lasers in photocoagulation are frequency-doubled Nd:YAG (532 nm), and yellow semiconductor laser (577 nm). The laser energy is absorbed primarily by melanin in the RPE and choroid, and by hemoglobin in blood. At a 532-nm wavelength approximately half of the laser energy incident on the retina is absorbed in the RPE, and the rest in the choroid.[25] The heat generated diffuses from the RPE and choroid into the retina and causes coagulation of the photoreceptors and, sometimes, of the inner retina. During 100-ms applications, the heat diffuses distances of up to 200 µm, thus "smoothing" the edge and extending the coagulated zone beyond the boundaries of the laser spot, termed "thermal blooming." Heat diffusion using shorter pulses and with smaller spot sizes can be limited to the photoreceptor layer, thereby avoiding the inner retinal damage.

The left panel in Figure 39.11A demonstrates the acute effects of an intense burn in a rabbit retina produced by 100 ms laser applications, including full-thickness injury and early necrotic features 24 hours after treatment. The left panel in Figure 39.11B demonstrates a light lesion produced by 15 ms pulses. Damaged photoreceptors are pyknotic, but the inner nuclear layer and ganglion cell layer are very well preserved.

Figure 39.12 illustrates the effect of laser power and pulse duration on the size of the coagulated zone in pigmented rabbits.[32] Table 39.2 lists the ratio of the lesion width to the retinal beam size for lesions of various clinical grades in human patients, as measured by optical coherence tomography (OCT) within 1 hour of treatment.[33] As can be seen, lesion size increases relative to the beam width with more intense lesions and longer pulses.

The threshold power required for the creation of retinal lesions increases with shorter pulses, since higher temperatures are required for coagulation during shorter exposures. An example of the threshold powers for lesions of various grades is plotted in Figure 39.13 as a function of pulse duration for a 132 µm retinal laser spot in the rabbit. A relatively modest power increase is required to produce comparable lesion grades going from 100 to 10 ms, whereas a much steeper increase is seen for durations under 10 ms. For pulse durations of 20, 50, and 100 ms, all the grades (mild, moderate, intense, very intense, and rupture) could be created with appropriate choice of power settings. At pulse durations below 10 ms, it became increasingly difficult to create intense lesions reproducibly without inadvertently rupturing the retina. At 2 ms or less it was not possible to create a moderate lesion reproducibly without rupturing the retina. At 1 ms, there was little or no difference between the power required to create a mild retinal lesion or produce a rupture.

The ratio of the threshold power required to produce a rupture to that required to produce a mild lesion is defined as the therapeutic window, and represents one means of quantifying the relative safety (dynamic range) of retinal photocoagulation. The larger this ratio, the greater the margin of safety to create a visible lesion without inadvertently inducing a retinal rupture. Figure 39.14 depicts the width of this therapeutic window as a function of pulse duration for two different laser spot sizes. For a 132 µm retinal laser beam size, as pulse duration decreases from 100 to 20 ms, the width of the therapeutic window declines from 3.9 to 3.0. When pulse duration is further decreased to 10 ms, the therapeutic window decreases further to 2.5, and it approaches unity at a pulse durations of 1 ms. For a 330 µm

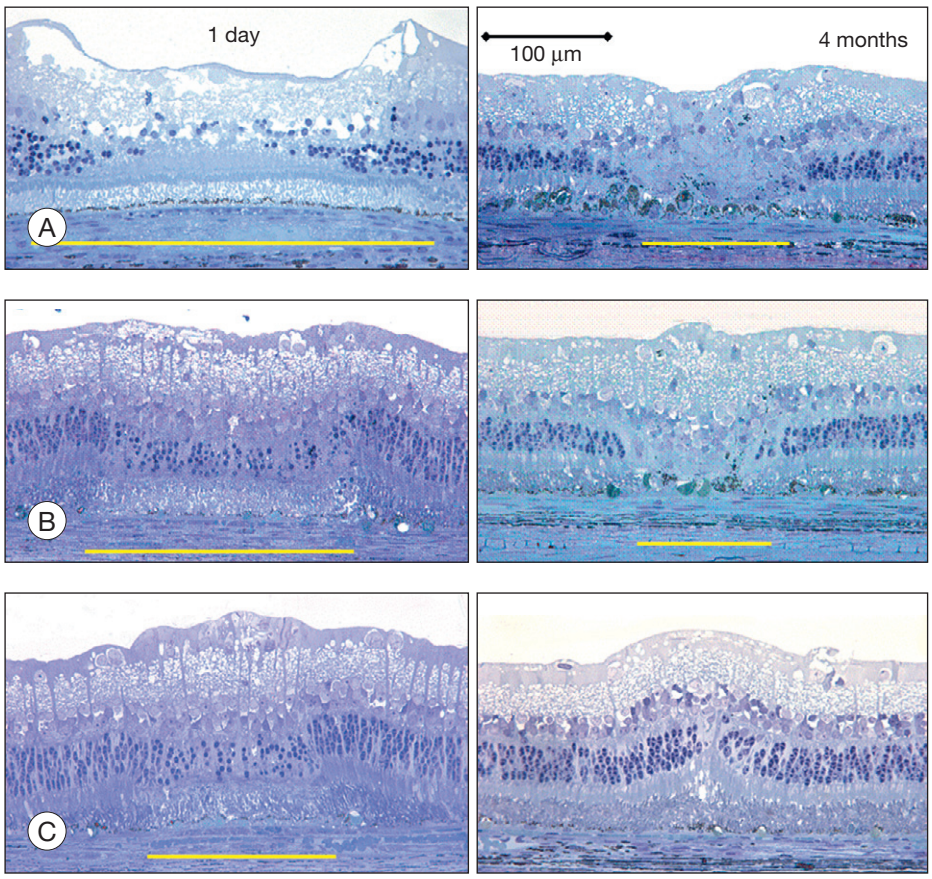

Fig. 39.11 Histology of the rabbit retina at 1 day (left column) and 4 months (right column) after photocoagulation. Retinal spot size is 330 µm, power 175 mW. (A) Intense retinal burn produced with 100 ms exposure. Yellow bar shows the lateral extent of the lesion. Note full-thickness retinal injury, including the inner retinal layers. (B) Light burn produced with 15 ms exposure. Photoreceptors are coagulated, while inner retina is well preserved. (C) Barely visible lesion produced with 7 ms pulse. Right column shows corresponding retinal scarring at 4 months. Note complete closure of the damage zone by shifting photoreceptors in the barely visible lesion.

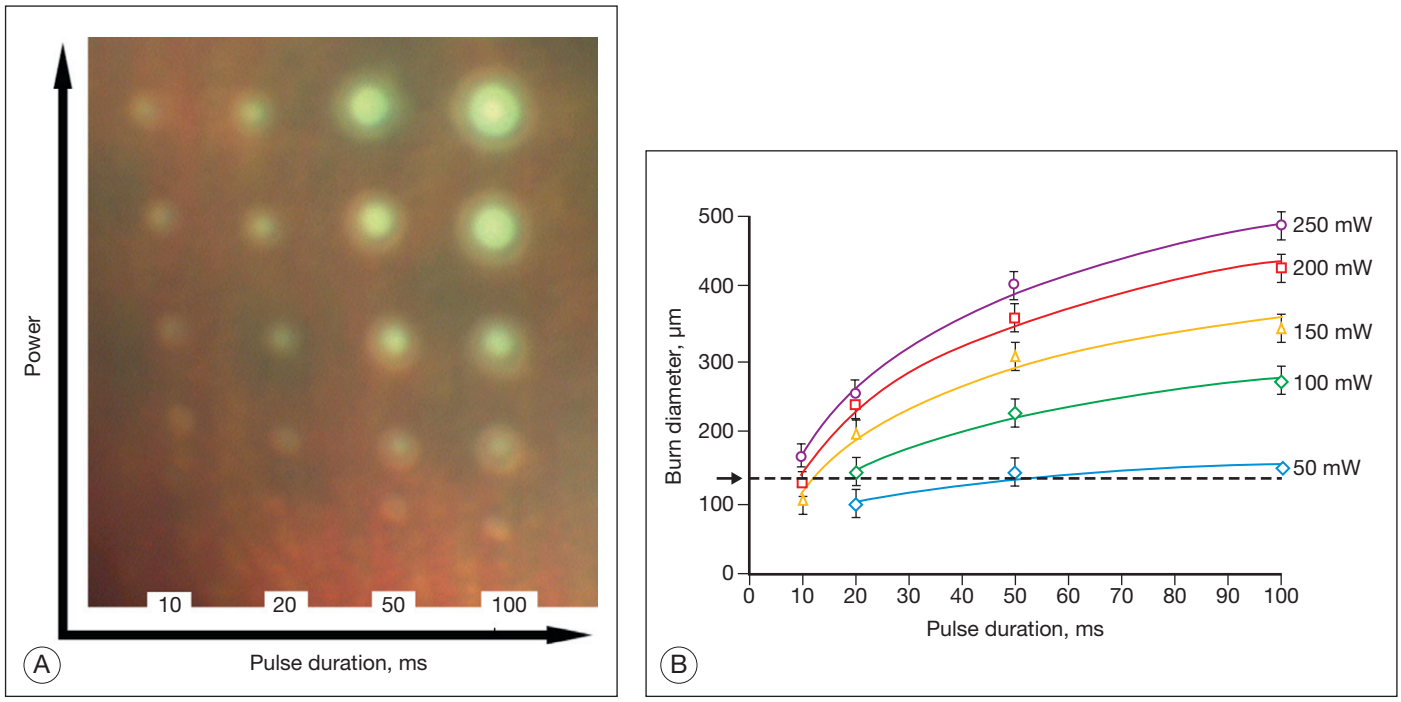

Fig. 39.12 (A) Retinal lesions in the rabbit eye with variable power and duration of exposure. Retinal beam size is 132 µm. (B) Lesion diameter as a function of laser power and duration of exposure. Laser beam size on the retina is 132 µm (indicated by dashed line and arrow).

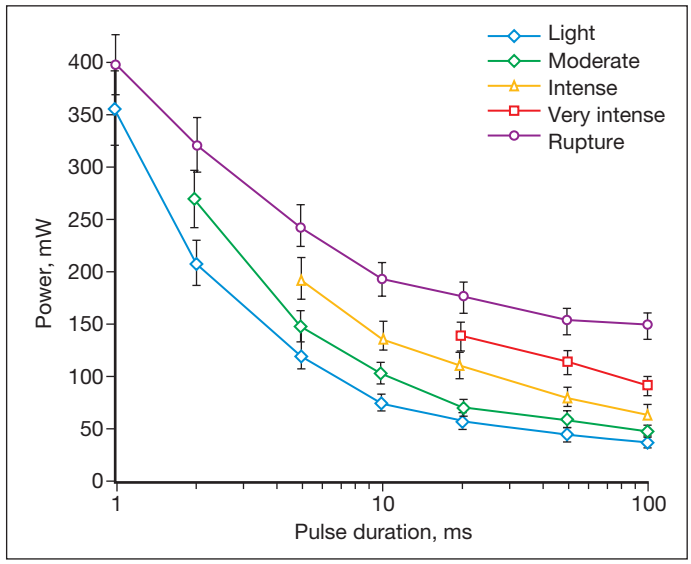

Fig. 39.13 Threshold power of retinal photocoagulation in rabbit eye, as a function of pulse duration. Laser beam size on the retina is 132 µm. Clinical grades indicated by the colors: light, moderate, intense, very intense, and rupture.

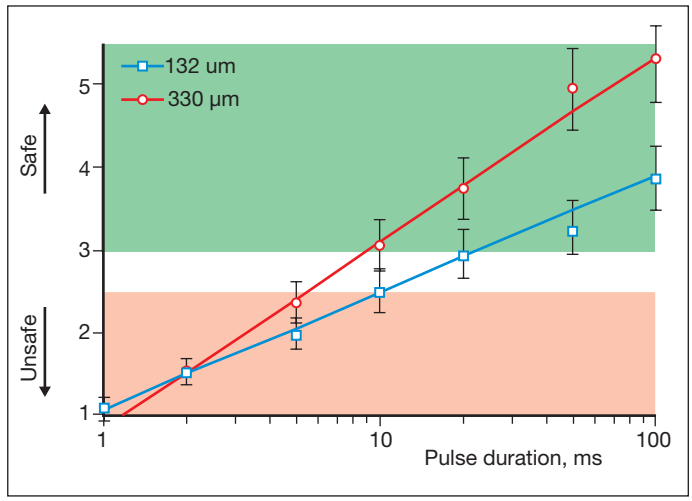

Fig. 39.14 Safe therapeutic window of retinal photocoagulation (ratio of the threshold of rupture to that of light coagulation) increases with pulse duration, and with a beam size on the retina (shown for 132 and 330 µm).

Table 39.2 Ratio of the lesion width to retinal beam size for various pulse durations and clinical grades, as measured by optical coherence tomography in human patients within 1 hour of application. Coagulation was performed with Area Centralis lens (laser beam magnification ×0.94)

Beam size		Lesion clinical grade					
In air	On retina	Moderate		Light		Barely visible	
		100 ms	20 ms	100 ms	20 ms	100 ms	20 ms
100 µm	94 µm	3.81 ± 0.98	2.50 ± 0.30		2.08 ± 0.24		
200 µm	188 µm	2.08 ± 0.22	1.49 ± 0.09		1.24 ± 0.08		0.93 ± 0.08
400 µm	376 µm	1.39 ± 0.08	1.15 ± 0.07	1.19 ± 0.11	0.99 ± 0.09	0.99 ± 0.08	0.74 ± 0.12

retinal laser spot size the therapeutic window declines from 5.4 to 3.7 to 3.1 when pulse durations decrease from 100 to 20 to 10 ms, respectively. With both spot sizes, the therapeutic window decreases to unity as pulse durations decrease to 1 ms. At this point there is effectively no safe range of retinal photocoagulation: mild lesion and rupture are equally likely to occur at the same power.

The width of the safe therapeutic window should suffice to accommodate for variations in fundus pigmentation, which typically do not exceed a factor of 2. To provide a safe therapeutic window larger than 2.5, pulse durations should equal or preferably exceed 10 ms for a beam of 330 μm, and 20 ms for the 132 μm spot size.

It is important to keep in mind that coagulation of blood vessels requires more energy than other tissue due to cooling by the blood flow. For example, if a spot size of 200 μm with exposure time of 200 ms is applied to occlude a blood vessel with flow velocity of 5 mm/s, the laser energy is effectively distributed over the column five times longer than the diameter of the laser spot. Thus the effective energy remaining at the photocoagulation site is five times lower than it would be in stationary tissue.

Healing of retinal lesions

Studies in rabbits demonstrate that in photocoagulation lesions the RPE layer is restored within a week, though its pigmentation may remain abnormal – either hyper- or hypopigmented.[34] In intense and moderate lesions gliotic scar filling the coagulated retinal layers stabilizes after 1 month, and the wound contracts to approximately 40% of the original lesion diameter, as shown in the right column in Figure 39.11A and B. However, in very light lesions (barely visible clinical grade), photoreceptors continue to shift into the damage zone and completely refill it by 4 months, as shown in Figure 39.11C, in the right panel. As a result, scarring and scotomata typically associated with conventional photocoagulation may be minimized or even completely avoided.[34] A similar phenomenon of restorative retinal plasticity has recently been observed in rats[35] and primates.[36] It is important to keep in mind, though, that in order to maintain clinical efficacy of photocoagulation with smaller and lighter lesions, a larger number of them should be applied, to keep the same total coagulated area.[33]

Pattern-scanning laser photocoagulation

The first attempts to make photocoagulation a completely automated procedure involved rather complex equipment, including image recognition software and eye tracking.[37] The complexity of such systems prevented their commercial introduction and acceptance in clinical practice.

A semiautomatic pattern-scanning photocoagulator (PASCAL, Topcon Medical Laser Systems) was introduced by OptiMedica in 2005.[38] It delivered patterns of laser spots, ranging from a single spot to 56 spots applied in a rapid sequence with a single depression of a foot pedal. The control of laser parameters was performed by means of a touch screen graphic user interface, facilitating selection of the different patterns of photocoagulation. The laser was activated by pressing a foot pedal, which was kept depressed until the entire pattern was completed, although it is possible for the physician to release the foot pedal and stop the laser at will, prior to completion of the pattern, if clinically indicated.

Patterns included square arrays with up to 5 × 5 spots, arcs with the number of concentric rows varying from 1 to 3, and circular patterns for photocoagulation of small holes and other lesions in the retinal periphery. Patterns for macular photocoagulation included rings and arcs with an adjustable central exclusion zone of up to 2 mm in diameter to allow for laser application, reducing the risk of inadvertent damage to the foveal avascular zone.

To deliver the whole pattern within the eye fixation time and avoid beam movement due to the ocular muscles, each exposure was required to be shorter than in conventional photocoagulation: 10–20 ms instead of 100–200 ms, traditionally applied with single spot exposures. Reduced heat diffusion into choroid during shorter exposures also resulted in patients experiencing less pain.[39–41] Short pulse lesions appear smaller and lighter than conventional burns produced with the same beam size, and therefore a larger number of them are required to treat the same total area.[33]

An automatic laser delivery, guided by diagnostic imaging and stabilized using eye tracking, has been recently introduced in a Navilase system (OD-OS). This system includes retinal image acquisition, annotation of the images to create a detailed treatment plan, and then automated delivery of the laser to the retina according to the treatment plan.

Clinical indications: treatment of diabetic retinopathy

Photocoagulation has proven safe and effective in the treatment of proliferative diabetic retinopathy. In this disorder the retina becomes ischemic and releases a variety of chemical messengers, most importantly, vascular endothelial growth factor (VEGF), that stimulate the growth of new blood vessels and also markedly increase retinal vascular permeability. The abnormal new vessels, associated fibrous tissue, and macular edema are major causes of the sight-threatening complications in diabetic eye disease. By destroying a portion of the peripheral retina with laser, it has been hypothesized that retinal metabolic demands and available nutrients are better balanced and the stimulus for growth of the new blood vessels is decreased. This treatment has been termed panretinal photocoagulation (Fig. 39.15) and significantly reduces the risk of vision loss due to neovascularization.

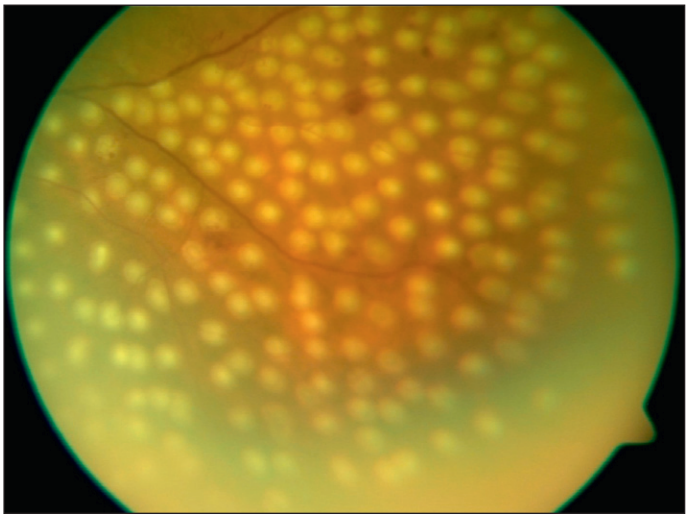

Fig. 39.15 Fundus photograph of a patient 1 week following application of panretinal photocoagulation with argon laser.

The side-effects of panretinal photocoagulation – mild nyctalopia and constriction of visual field – are felt to be outweighed by the preservation of the central vision, and have been confirmed in multiple large randomized clinical trials.[42] Similarly, the focal laser photocoagulation to actively leaking microaneurysms, and the grid photocoagulation to areas of diffuse retinal permeability (Fig. 39.16) have been shown to reduce clinically significant macular edema associated with diabetic retinopathy and slow the rate of vision loss. These effects have been confirmed in large randomized multicenter clinical trials.[43]

Age-related macular degeneration: extrafoveal neovascular lesions

Another application for laser photocoagulation in the past was for the treatment of extrafoveal CNV membranes that occur in AMD. Intense photocoagulation that destroyed the invading vascular membrane usually leaves a chorioretinal scar and a blind spot or scotoma, but if the lesions treated were outside the center of the macula, the treatment was typically well tolerated by the patients. Currently, many physicians have elected to use PDT as an alternative to intense focal photocoagulation, or to use anti-VEGF therapy, because of later recurrences and eventual spread of lesions into the macula.

Additional applications of retinal photocoagulation include grid and focal treatment of leaking microvascular abnormalities, in branch vein occlusion and radiation retinopathy; and treatment of retinal breaks and lattice degeneration to prevent retinal detachment.

Selection of optimal wavelengths for coagulation

A number of important factors must be considered when choosing the best wavelength for a particular photocoagulation application. The first consideration is to determine what absorbers are present in the site to be photocoagulated. Wavelengths that are highly absorbed by macular yellow (such as 488 nm) are relatively contraindicated when treating in or near the macula.

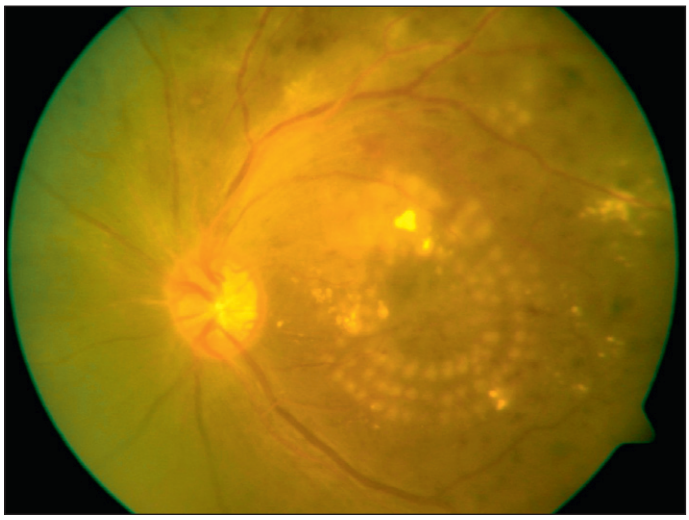

Fig. 39.16 Fundus photograph of a patient with clinically significant macular edema including central macular thickening and paramacular lipid exudates 1 week following grid photocoagulation. Note concentric rows of photocoagulation spots surrounding the macula, best seen inferiorly.

Absorption of these wavelengths in macular pigments may cause heating and destruction of the nerve fiber layer, resulting in loss of vision. As shown in Figure 39.1B, in the macular region, wavelengths longer than 500 nm should be chosen, such as the green argon (514 nm) or the frequency-doubled YAG (532 nm) or semiconductor yellow (577 nm) laser. Melanin provides good absorption at most photocoagulation wavelengths. Wavelength selection is therefore less important when melanin is the primary absorber. To minimize scattering loss in cataract or in vitreous opacities the longer wavelengths (yellow, 577 nm, or red, 640–680 nm) are efficacious. If scattering by the ocular tissues is not significant, the argon green or doubled YAG continues to serve well.

When hemoglobin is the primary absorber (Fig. 39.1B), as in the treatment of vascularized tumors, a wavelength shorter than 600 nm is preferable. Treatment of CNV may be effective using red light through indirect heat transfer from the surrounding melanin. In general, when photocoagulating structures contain a large quantity of hemoglobin, wavelengths between 520 and 580 nm are best suited. Ideally, for coagulation of blood vessels the photon penetration depth should be similar to the vessel diameter, thus providing uniform heating of the blood vessel without superficial damage and perforation.

Tunable lasers may provide the flexibility to select a wavelength of choice for required photothermal procedure. However, tunable lasers are more costly, require more maintenance, and are now less commonly employed clinically than previously.

Photodisruption

When tissue temperature exceeds the vaporization threshold vapor bubbles are produced, which may lead to rupture of the tissue within a zone comparable to the bubble size. This process of explosive vaporization is typically employed for tissue dissection. The actual temperature required for vaporization varies between 100 and 305°C depending on pulse duration and on presence of the bubble nucleation sites.[44] For efficient heating of tissue the pulse energy should be delivered fast enough to avoid heat diffusion from the laser absorption zone during the pulse, a condition called "thermal confinement." In other words, the laser pulse duration should be shorter than the heat relaxation time, or the time of heat diffusion from the zone of laser absorption, L: $\tau < L^2/4\alpha$, where L is the penetration depth of light in tissue ($L = 1/\mu_a$), and α is thermal diffusivity of tissue. For example, with light penetration depth of 1 μm, pulse durations should not exceed 1.7 μs. In this case the temperature rise ΔT in tissue with absorption coefficient μ_a achieved during laser pulse with duration τ at irradiance I (W/cm^2) is: $\Delta T = \frac{\mu_a \cdot I \cdot \tau}{\rho \cdot c}$, where ρ and c are tissue density and heat capacity. A higher absorption coefficient μ_a facilitates reaching a vaporization threshold with a lower total energy deposition ($E_{tot} = I\tau$). Precise tissue ablation requires the use of laser wavelengths corresponding to a small optical penetration depth in tissue in order to confine the energy deposition to a small volume.

Much shorter pulses may produce stress confinement, i.e., conditions when an acoustic wave produced due to thermal expansion of the material cannot escape from the heated zone during the laser pulse. Since the velocity of sound in water is about 1.5 km/s, the stress confinement conditions are achieved within the 1 μm penetration depth if pulse duration does not exceed 0.7 ns. In such conditions powerful stress waves may be

generated which propagate with supersonic velocities and may result in significant damage to tissue, such as disruption and fragmentation.[44]

Vaporization of water in an overheated volume results in the formation of a short-living vapor bubble (a so-called cavitation bubble) which expands, cools down, and collapses during the time determined by its radius at maximal expansion. The lifetime of the spherical cavity with radius R_0 in free nonviscous liquid is described by the Rayleigh equation: $\tau = 0.91R_0\sqrt{\frac{\rho}{P_0}}$, where ρ is liquid density and P_0 is ambient pressure.[45] For example, in water at atmospheric pressure, a cavity of 0.1 mm in radius collapses in about 10 μs. (Growth and collapse of a spherical bubble take approximately the same time.) Symmetric collapse of a spherical cavity may lead to overheating of the liquid and formation of the secondary bubble. Due to the short lifetime these bubbles are not visible to the eye during surgery, but they can be easily visualized using fast flash photography. As shown in Figure 39.17, at the liquid–tissue interface the bubble might be deformed, and the secondary bubble may not be created. Importantly, a collapsing cavitation bubble at the fiber probe or next to the tissue surface may produce a water jet which is capable of damaging tissue at distances exceeding the bubble radius by a factor of 4.[46,47]

Explosive vaporization can be produced by absorption of laser radiation in water or in tissue. Strong absorption in water can be achieved at mid-infrared wavelengths. For example, penetration of the Er:YAG laser (λ = 2.94 mm) in water is about 1 μm. Shallow penetration of these lasers necessitates the fiber-based delivery of this light into a liquid medium. A thin layer of water in front of the intraocular probe is overheated with the laser pulse, and the resulting vaporization leads to rupture of tissue in proximity to the probe. The best implementation of this principle has been achieved with Er:YAG-based dissection of epiretinal membranes[48,49] (Fig. 39.18). Since a burst of closely spaced pulses, rather than a single pulse, was applied in that device, the actual vapor bubble had an elliptical shape and extended several hundreds of microns from the probe.[50]

Alternatively, overheating of liquid can be achieved with a laser strongly absorbed in the tissue constituents. For example, a fiber-delivered ArF excimer laser (λ = 193 nm), which is strongly absorbed by proteins (penetration depth 0.2 μm in

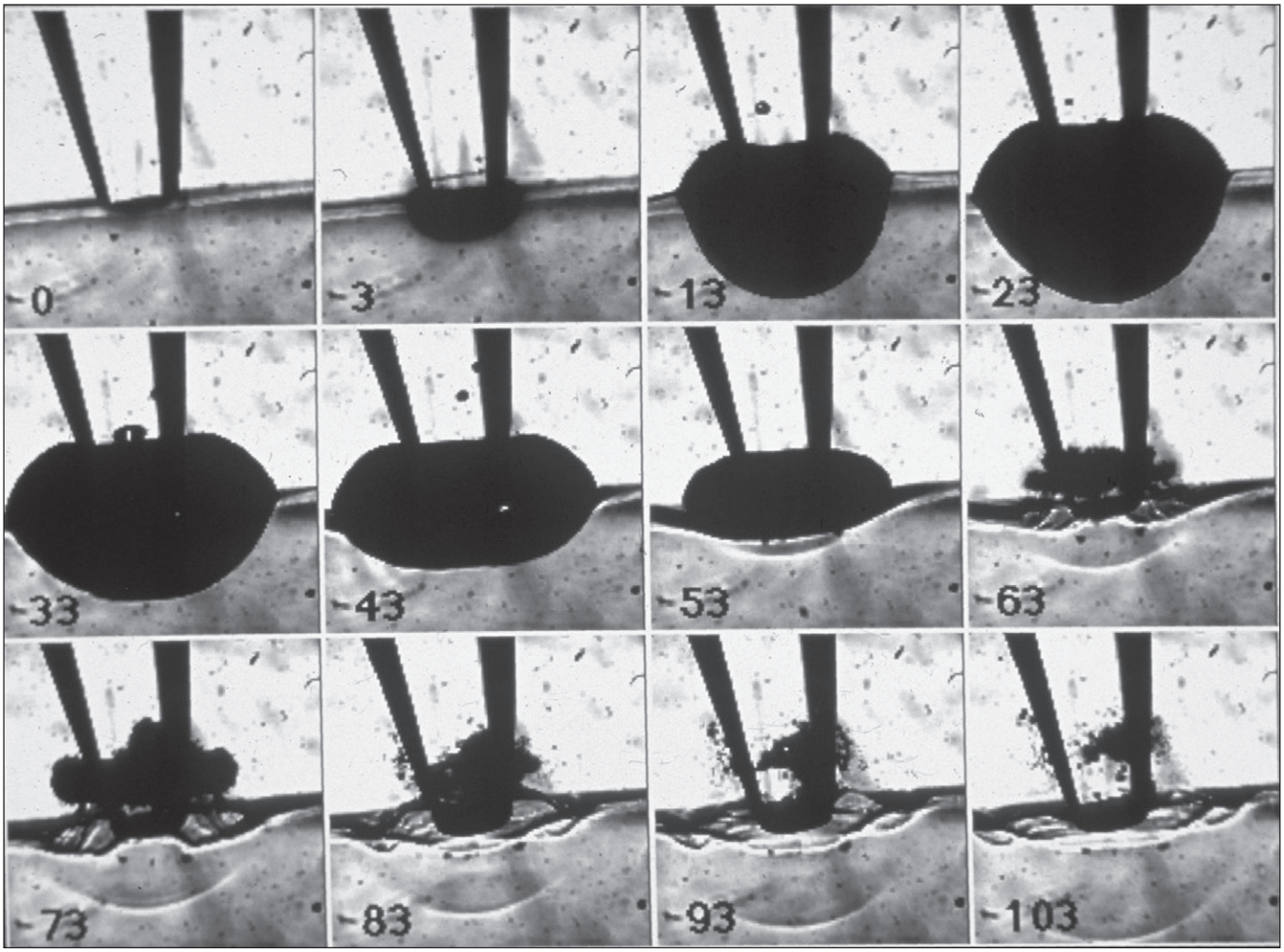

Fig. 39.17 Dynamics of the cavitation bubble at the gelatin–saline interface observed with fast flash photography. Bubble is created by a pulse of ArF excimer laser delivered via the tapered optical fiber. Numbers in each frame indicate a delay in microseconds between the laser pulse (10 ns) and a microsecond-long flash.

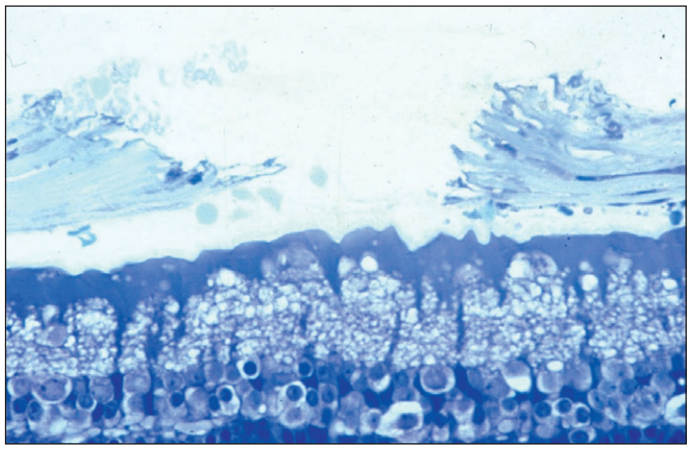

Fig. 39.18 Epiretinal membrane dissected by the Er:YAG laser. Note the absence of retinal damage despite its close proximity.

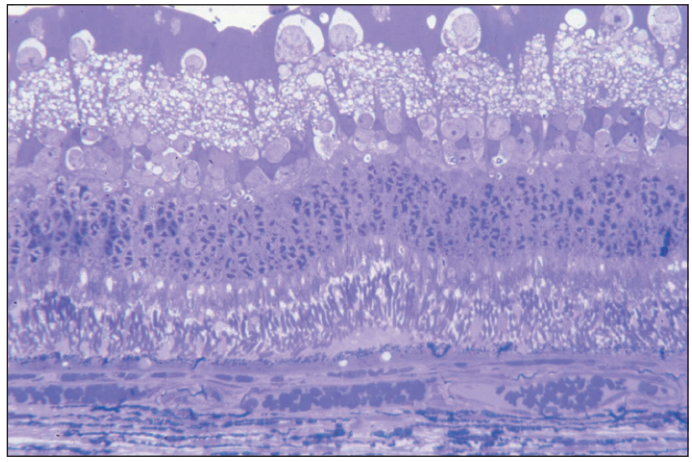

Fig. 39.19 Rabbit retina 24 hours after selective retina therapy with infrared semiconductor laser. Note that damage is almost exclusively confined to the retinal pigment epithelial (RPE) layer with preservation of the outer nuclear layer and even the outer segments of overlying photoreceptors. There is a small localized effusion between the RPE and photoreceptors.

tissue), has been applied for dissection of epiretinal and subretinal membranes.[51,52] In this case the laser light overheats the tissue and leads to vaporization of its water content with subsequent tissue rupturing.[53,54] Despite the early promise of both of these devices (Er:YAG and ArF excimer lasers) in clinical tests, both have failed to achieve widespread acceptance in medical practice due in part to cost, the rigidity of the fibers, and the lack of coagulation capability.

Another approach to dissection of transparent tissue utilizes ionization of the material and formation of plasma from a high-intensity laser beam. At extremely high irradiances (10^8-10^{11} W/cm^2), that can be achieved in a short-pulsed (ns–fs) tightly focused laser beam, transparent material can be ionized and ions absorbing the laser light reach very high temperatures.[55] This mechanism, called dielectric breakdown, allows for a very localized deposition of energy in the middle of a transparent liquid or solid – at the focal point of the laser beam. This process is widely used in fragmentation of the opacified posterior lens capsule (secondary cataract) with nanosecond Nd:YAG lasers. At shorter pulse durations (1 ps–100 fs) and lower energies, this process is applied to intrastromal ablation – formation of a corneal flap for refractive surgery.[56,57] This approach has also been tested in the dissection of epiretinal membranes using the tightly focused beam directed from outside the eye.[58] Despite the fact that very low energy is required for this process (several microjoules with ps lasers), its applicability in the posterior pole is limited due to the difficulty in axial differentiation between the epiretinal membranes and the retina located very close behind them. In addition, strong optical aberrations in the periphery of the posterior pole preclude tight focusing of the laser beam in these areas.

Selective retina therapy (SRT)

Light is strongly absorbed in the melanosomes in the RPE ($\mu_a \approx 8000$ cm^{-1}).[59] The application of short (submicrosecond) laser pulses allows for confinement of the thermal and mechanical effects of this absorption within the RPE layer, thus sparing the photoreceptors and the inner retina[60,61] (Fig. 39.19). It has been demonstrated that the application of repetitive pulses of microsecond and submicrosecond duration results in selective damage to RPE, presumably due to the formation of small cavitation bubbles around melanosomes.[59] Subsequent RPE proliferation and migration restore continuity of the RPE layer. Several small clinical studies have shown the efficacy of SRT in diabetic maculopathy, central serous choroidopathy,[62,63] and subfoveal fluid after rhegmatogenous retinal detachment.[64,65] Despite its clinical promise, this technique has not been commercialized. One of the difficulties with SRT is the lack of visible change in the retinal appearance, making it difficult to assess adequate laser dosimetry as the applications are being placed. An acousto-optical system is currently under development that may help to assess the threshold energy density required for cavitation in RPE.[66] An alternative approach to SRT is the rapid scanning of a laser beam providing microsecond exposures, sufficiently short for selective treatment of the RPE.[67,68]

FUTURE DEVELOPMENTS

Monitoring retinal temperature

Retinal thermal therapies with temperature rise below the threshold of immediately visible tissue response, such as sublethal hyperthermia, do not have as high a degree of predictability as conventional thermal photocoagulation methods. For successful sublethal treatment the temperature rise in tissue is on the order of 10°C.[69] However, due to the strong variation in fundus pigmentation the light absorption varies from patient to patient, and even between different areas in the same eye. Therefore the same irradiation settings may lead to very different results in different patients, and so direct measurement of retinal temperature during such treatments is highly desirable. Similarly, it would be desirable to monitor retinal temperature in the treated spot during photocoagulation to provide uniform outcomes in areas with different pigmentation.

A noninvasive method of determination of retinal temperature has been developed, which is based on the detection of acoustic waves generated in RPE by short laser pulses.[70] An acoustic transducer for the detection of the pressure waves is built into a contact lens attached to the treated eye during the procedure. The pressure waves are generated due to thermoelastic expansion of melanosomes upon absorption of the short (submicrosecond) laser pulses. The key issue in this approach is that the thermoelastic expansion coefficient of water varies

with temperature, by about 1% per 1°C.[70] This effect allows for monitoring the changes in temperature of the RPE cells by monitoring the changes in amplitude of acoustic waves generated by the laser pulses of constant energy. The probing laser pulses are applied simultaneously with application of a therapeutic laser to detect temperature rise in tissue during the exposure. It has been demonstrated that precision of this method is on the order of 1°C. Clinical testing of the system is currently in progress.

Optical monitoring of tissue changes in real time

An optical approach to real-time feedback during retinal photocoagulation has recently been demonstrated.[71] It is based on OCT monitoring of the heated tissue expansion and changes in retinal scattering during coagulation. The system operates with ms temporal resolution, which should be fast enough for real-time monitoring of retinal photocoagulation.

Another technique for detection of tissue condition during slow thermal therapy is based on spectroscopy of white light scattered from the tissue.[72] Cellular response to thermal stress involves expression of various proteins, as well as changes in their aggregation and concentration. All these effects result in changes of the refractive indices and/or the sizes and shapes of the cellular organelles, which can be detected using light-scattering spectroscopy. Particle sizes down to 100 nm in diameter can be detected using light within the spectral range of 350–1000 nm.[72] Since the information is obtained optically and without any staining this technique operates in real time and is noninvasive. It has been observed that scattering coefficients of some organelles change very strongly (up to 70%) and rapidly (20 seconds) in the heated cells.[73]

REFERENCES

1. Meyer-Schwickerath G. Light coagulation. St Louis: Mosby; 1960.
2. Palanker DV, Blumenkranz MS, Marmor MF. 50 years of ophthalmic laser therapy. Arch Ophthalmol 2011;129:1613–9.
3. Smith G, Atchinson DA. The eye and visual optical instruments. Cambridge: Cambridge University Press; 1996, chapter 13.
4. Thompson KP, Ren QS, Parel J-M. Therapeutic and diagnostic application of lasers in ophthalmology. In: Waynant RW, editor. Lasers in medicine. Boca Raton FL: CRC Press; 2002, chapter 8.
5. Pomerantzeff O, Pankratov M, Wang GJ, et al. Wide-angle optical-model of the eye. Am J Optom Phys Opt 1984;61:166–76.
6. Walsh G, Charman WN, Howland HC. Objective technique for the determination of monochromatic aberrations of the human eye. J Opt Soc Am A 1984;1: 987–92.
7. Doornbos RMP, Lang R, Aalders MC, et al. The determination of in vivo human tissue optical properties and absolute chromophore concentrations using spatially resolved steady-state diffuse reflectance spectroscopy. Phys Med Biol 1999;44:967–81.
8. Troy TL, Thennadil SN. Optical properties of human skin in the near infrared wavelength range of 1000 to 2200 nm. J Biomed Opt 2001;6:167–76.
9. Dougherty TJ, Mang TS. Characterization of intra-tumoral porphyrin following injection of hematoporphyrin derivative or its purified component. Photochem Photobiol 1987;46:67–70.
10. Schmidt U, Birngruber R, Hasan T. [Selective occlusion of ocular neovascularization by photodynamic therapy.] Ophthalmologe 1992;89:391–4.
11. Miller H, Miller B. Photodynamic therapy of subretinal neovascularization in the monkey eye. Arch Ophthalmol 1993;111:855–60.
12. Kramer M, Miller JW, Michaud N, et al. Liposomal benzoporphyrin derivative verteporfin photodynamic therapy. Selective treatment of choroidal neovascularization in monkeys. Ophthalmology 1996;103:427–38.
13. Miller JW, Walsh AW, Kramer M, et al. Photodynamic therapy of experimental choroidal neovascularization using lipoprotein-delivered benzoporphyrin. Arch Ophthalmol 1995;113:810–8.
14. Woodburn KW, Engelman CJ, Blumenkranz MS. Photodynamic therapy for choroidal neovascularization: a review. Retina 2002;22:391–405;.
15. Birngruber R, Indorf L, Soultanopoulos D, et al. Photodynamic occlusion of ocular neovascularization: Preclinical evaluation of liposomal zinc phthalocyanine. Invest Ophthalm Vis Sci 1996;37:4214–4214.
16. Arnold J, Kilmartin D, Olson J, et al. Verteporfin therapy of subfoveal choroidal neovascularization in age-related macular degeneration: Two-year results of a randomized clinical trial including lesions with occult with no classic choroidal neovascularization-verteporfin in photodynamic therapy report 2. Am J Ophthalmol 2001;131:541–60.
17. Luttrull JK, Musch DC, Mainster MA. Subthreshold diode micropulse photocoagulation for the treatment of clinically significant diabetic macular oedema. Br J Ophthalmol 2005;89:74–80.
18. Figueira J, Khan J, Nunes S, et al. Prospective randomised controlled trial comparing sub-threshold micropulse diode laser photocoagulation and conventional green laser for clinically significant diabetic macular oedema. Br J Ophthalmol 2009;93:1341–4.
19. Luttrull JK, Musch DC, Mainster MA. Subthreshold diode micropulse photocoagulation for the treatment of clinically significant diabetic macular oedema. Br J Ophthalmol 2005;89:74–80.
20. Luttrull JK, Musch DC, Spink CA. Subthreshold diode micropulse panretinal photocoagulation for proliferative diabetic retinopathy. Eye (Lond) 2008;22: 607–12.
21. Ohkoshi K, Yamaguchi T. Subthreshold micropulse diode laser photocoagulation for diabetic macular edema in Japanese patients. Am J Ophthalmol 2010; 149:133–9.
22. Desmettre TJ, Mordon SR, Buzawa DM, et al. Micropulse and continuous wave diode retinal photocoagulation: visible and subvisible lesion parameters. Br J Ophthalmol 2006;90:709–12.
23. Luttrull JK, Sramek C, Palanker D, et al. Long-term safety, high-resolution imaging, and tissue temperature modeling of sub-visible diode micropulse photocoagulation for retinovascular macular edema. Retina 2011;epub ahead of print.
24. Niemz M. Laser–tissue interactions. Fundamentals and applications. Berlin: Springer; 2002.
25. Sramek C, Paulus Y, Nomoto H, et al. Dynamics of retinal photocoagulation and rupture. J Biomed Optics 2009;14:034007–13.
26. Oosterhuis JA, Journeedekorver HG, Kakebeekekemme HM. Transpupillary thermotherapy in choroidal melanomas. Arch Ophthalmol 1995;113:693–693.
27. Reichel E, Berrocal AM, Ip M, et al. Transpupillary thermotherapy of occult subfoveal choroidal neovascularization in patients with age-related macular degeneration. Ophthalmology 1999;106:1908–14.
28. Newsom RSB, McAlister JC, Saeed M, et al. Transpupillary thermotherapy (TTT) for the treatment of choroidal neovascularisation. Br J Ophthalmol 2001;85:173–8.
29. Svaasand LO. Laser-induced hyperthermia – physics considerations and limitations. Laser Surg Med 1988;8:182–182.
30. Svaasand LO, Gomer CJ, Profio AE. Laser-induced hyperthermia of ocular tumors. Appl Optics 1989;28:2280–7.
31. Mainster MA, Reichel E. Transpupillary thermotherapy for age-related macular degeneration: Long-pulse photocoagulation, apoptosis, and heat shock proteins. Ophthalmic Surg Las 2000;31:359–73.
32. Jain A, Blumenkranz MS, Paulus Y, et al. Effect of pulse duration on size and character of the lesion in retinal photocoagulation. Arch Ophthalmol 2008;126:78–85.
33. Palanker D, Lavinsky D, Blumenkranz MS, et al. The impact of pulse duration and burn grade on size of retinal photocoagulation lesion: implications for pattern density. Retina 2011;31:1664–9.
34. Paulus YM, Jain A, Gariano RF, et al. Healing of retinal photocoagulation lesions. Invest Ophthalmol Vis Sci 2008;49:5540–5.
35. Belokopytov M, Belkin M, Dubinsky G, et al. Development and recovery of laser-induced retinal lesion in rats. Retina 2010;30:662–70.
36. Merigan WH, Strazzeri J, DiLoreto DA, Jr, et al. Visual recovery after outer retinal damage in the macaque. Invest Ophthalmol Vis Sci 2011;52:3202.
37. Wright CHG, Barrett SF, Ferguson RD, et al. Initial in vivo results of a hybrid retinal photocoagulation system. J Biomed Opt 2000;5:56–61.
38. Blumenkranz MS, Yellachich D, Andersen DE, et al. Semiautomated patterned scanning laser for retinal photocoagulation. Retina 2006;26:370–6.
39. Nagpal M, Marlecha S, Nagpal K. Comparison of laser photocoagulation for diabetic retinopathy using 532-nm standard laser versus multispot pattern scan laser. Retina 2010;30:452–8.
40. Muqit MM, Marcellino GR, Gray JC, et al. Pain responses of Pascal 20 ms multispot and 100 ms single-spot panretinal photocoagulation: Manchester Pascal Study, MAPASS report 2. Br J Ophthalmol 2010;94:1493–8.
41. Muqit MM, Gray JC, Marcellino GR, et al. In vivo laser–tissue interactions and healing responses from 20- vs 100-millisecond pulse Pascal photocoagulation burns. Arch Ophthalmol 2010;128:448–55.
42. DRS Study Group. Photocoagulation treatment for proliferative diabetic retinopathy. clinical application of DRS findings, DRS report number 8. Ophthalmology 1981;88:583–600.
43. ETDRS Study Group. Early Photocoagulation for Diabetic Retinopathy. ETDRS report number 9. Ophthalmology 1991;98:766–85.
44. Vogel A, Venugopalan V. Mechanisms of pulsed laser ablation of biological tissues. Chem Rev 2003;103:2079–2079.
45. Young FR. Cavitation. Maidenhead: McGraw-Hill; 1989. p. 13–6.
46. Palanker D, Vankov A, Miller J. Effect of the probe geometry on dynamics of cavitation. SPIE, Laser–Tissue Interaction XIII 2002;4617:112–7.
47. Palanker D, Vankov A, Miller J, et al. Prevention of tissue damage by water jet during cavitation. J Appl Phys 2003;94:2654–61.
48. D'Amico DJ, Blumenkranz MS, Lavin MJ, et al. Multicenter clinical experience using an erbium:YAG laser for vitreoretinal surgery. Ophthalmology 1996;103:1575–85.
49. D'Amico DJ, Brazitikos PD, Marcellino GR, et al. Initial clinical experience with an erbium:YAG laser for vitreoretinal surgery. Am J Ophthalmol 1996;121: 414–25.

50. Lin CP, Stern D, Puliafito CA. High-speed photography of Er: YAG laser ablation in fluid. Implication for laser vitreous surgery. Invest Ophthalmol Vis Sci 1990;31:2546–50.
51. Palanker D, Hemo I, Turovets I, et al. Vitreoretinal ablation with the 193-nm excimer laser in fluid media. Invest Ophthalmol Vis Sci 1994;35:3835–40.
52. Hemo I, Palanker D, Turovets I, et al. Vitreoretinal surgery assisted by the 193-nm excimer laser. Invest Ophthalmol Vis Sci 1997;38:1825–9.
53. Palanker D, Turovets I, Lewis A. Mechanisms of tissue damage during ArF excimer endolaser microsurgery. Laser–Tissue Interaction VII, Proc SPIE 1996;2681:220–5.
54. Palanker D, Turovets I, Lewis A. Dynamics of ArF excimer laser-induced cavitation bubbles in gel surrounded by a liquid medium. Lasers Surg Med 1997;21:294–300.
55. Vogel A, Busch S, Jungnickel K, et al. Mechanisms of intraocular photodisruption with picosecond and nanosecond laser pulses. Lasers Surg Med 1994;15:32–43.
56. Krueger RR, Quantock AJ, Juhasz T, et al. Ultrastructure of picosecond laser intrastromal photodisruption. J Refract Surg 1996;12:607–12.
57. Yen KG, Sachs Z, Elner VE, et al. Histopathology of femtosecond laser intrastromal refractive surgery in rabbits. Invest Ophthalmol Vis Sci 1999;40: S621–S621.
58. Cohen BZ, Wald KJ, Toyama K. Neodymium:YLF picosecond laser segmentation for retinal traction associated with proliferative diabetic retinopathy. Am J Ophthalmol 1997;123:515–23.
59. Brinkmann R, Huttmann G, Rogener J, et al. Origin of retinal pigment epithelium cell damage by pulsed laser irradiance in the nanosecond to microsecond time regimen. Laser Surg Med 2000;27:451–64.
60. Roider J, Hillenkamp F, Flotte T, et al. Microphotocoagulation: selective effects of repetitive short laser pulses. Proc Natl Acad Sci U S A 1993;90:8643–7.
61. Roider J, Michaud NA, Flotte TJ, et al. Response of the retinal pigment epithelium to selective photocoagulation. Arch Ophthalmol 1992;110:1786–92.
62. Roider J, Brinkmann R, Wirbelauer C, et al. Subthreshold (retinal pigment epithelium) photocoagulation in macular diseases: a pilot study. Br J Ophthalmol 2000;84:40–7.
63. Elsner H, Porksen E, Klatt C, et al. Selective retina therapy in patients with central serous chorioretinopathy. Graefes Arch Clin Exp Ophthalmol 2006;244:1638–45.
64. Koinzer S, Elsner H, Klatt C, et al. Selective retina therapy (SRT) of chronic subfoveal fluid after surgery of rhegmatogenous retinal detachment: three case reports. Graefes Arch Clin Exp Ophthalmol 2008;246:1373–8.
65. Brinkmann R, Roider J, Birngruber R. Selective retina therapy (SRT): a review on methods, techniques, preclinical and first clinical results. Bull Soc Belge Ophtalmol 2006;51–69.
66. Brinkmann R, Schuele G, Joachimmeyer E, et al. Determination of absolute fundus temperatures during retinal laser photocoagulation and selective RPE treatment. Invest Ophthalmol Vis Sci 2001;42:S696–S696.
67. Framme C, Alt C, Schnell S, et al. Selective targeting of the retinal pigment epithelium in rabbit eyes with a scanning laser beam. Invest Ophthalmol Vis Sci 2007;48:1782–92.
68. Paulus YM, Jain A, Nomoto H, et al. Selective retinal therapy with microsecond exposures using a continuous line scanning laser. Retina 2011. 31:380–8.
69. Sramek C, Mackanos M, Spitler R, et al. Non-damaging retinal phototherapy: dynamic range of heat shock protein expression. Invest Ophthalmol Vis Sci 2010;52:1780–7.
70. Schule G, Huttmann G, Framme C, et al. Noninvasive optoacoustic temperature determination at the fundus of the eye during laser irradiation. J Biomed Opt 2004;9:173–9.
71. Huttmann G, Müller H, Schlott K, et al. Investigating of retinal photocoagulation by high-speed OCT in rabbits. Invest Ophthalmol Vis Sci 2011;52: 549–.
72. Fang H, Ollero M, Vitkin E, et al. Noninvasive sizing of subcellular organelles with light scattering spectroscopy. IEEE J Sel Top Quant 2003;9:267–76.
73. Schuele G, Huie P, Vankov A, et al. Non-invasive monitoring of the thermal stress in RPE using light scattering spectroscopy. Ophthalm Technol SPIE Proc 2004;5314.